Electronic Supplementary Material (ESI) for Dalton Transactions.

Supporting information for

Probing the validity of the spinel inversion model: A combined SPXRD, PDF, EXAFS and NMR study of $ZnAl_2O_4$

Sanna Sommer,[a] Espen Drath Bøjesen,[b] Nina Lock,[c] Hidetaka Kasai,[d] Jørgen Skibsted,[e] Eiji Nishibori, [d] Bo Brummerstedt Iversen[a]*

Table of Contents

PXRD Simulations

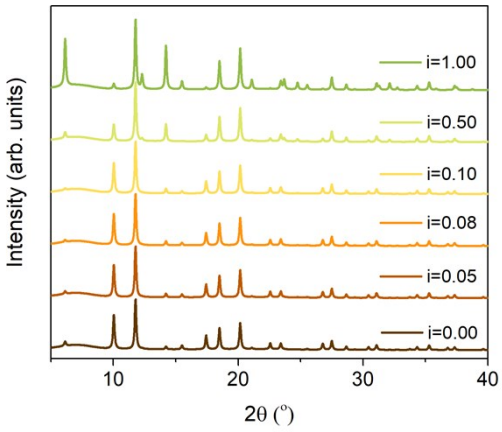

Figure S1. Simulated PXRD patterns for various degrees of inversion of the cations, based on the S1 peak broadening and background description. The occupancy of the interstitial sites *48f* and *16c* are 0 while the occupancy for oxygen on the spinel 32e site is 1. The simulations demonstrate how the defects influence the relative peak intensities.

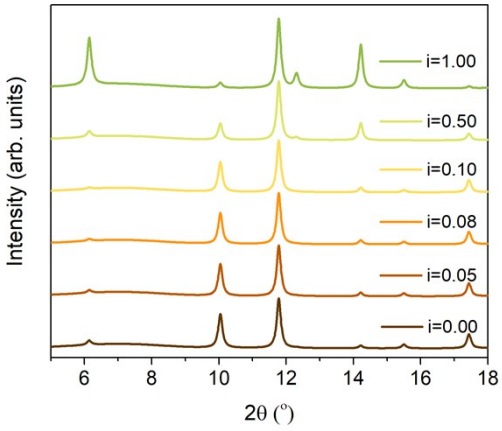

Figure S2. Zoom of Fig. S1.

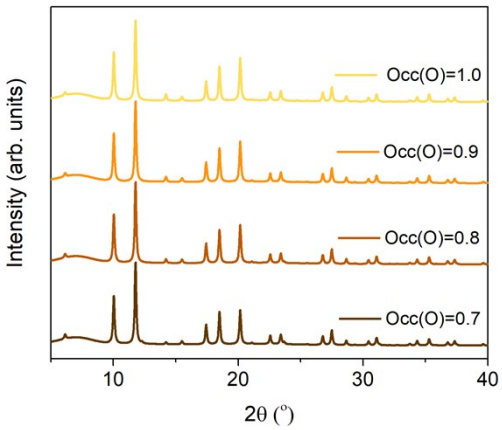

Figure S3. Simulated PXRD patterns for varying degrees of oxygen occupancies on the *32e* spinel site. The simulations are based on the S1 peak broadening and background description. The occupancy of the interstitial sites *48f* and *16c* are 0. The degree of inversion is set to 0.077% according to ^{27}Al NMR data (Table S1). Due to the low scattering power of O, only limited changes are observed in the diffraction pattern.

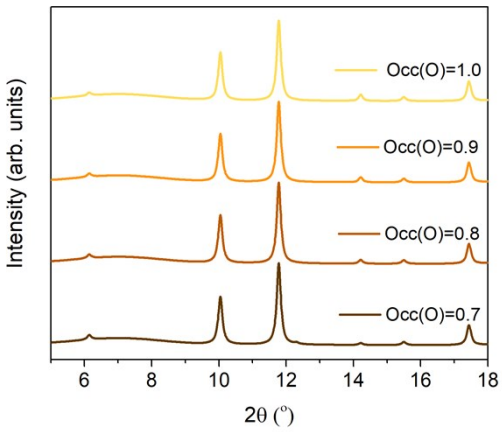

Figure S4. Zoom of Fig. S3.

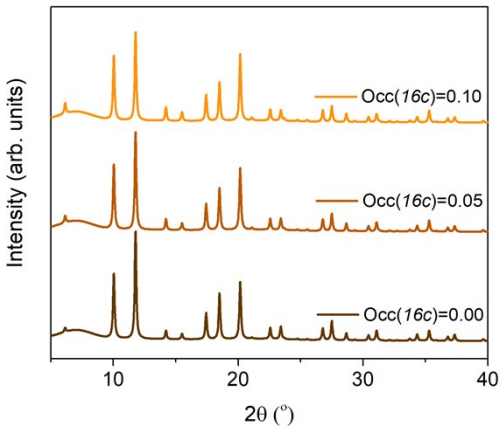

Figure S5. Simulated PXRD patterns for varying degrees of occupancy on the *16c* (0, 0, 0) interstitial site, assuming Zn on the site. The simulations are based on the S1 peak broadening and background description. The occupancy of the interstitial *48f* site is 0. The degree of inversion is set to 0.077% according to ^{27}AlNMR data (Table S1). Occupancy on this site mostly influence the peaks at 6° and 14.2°. These peaks are also highly influenced by the degree of inversion (Fig. S1) and occupancy on the *48f* site (Figure S7).

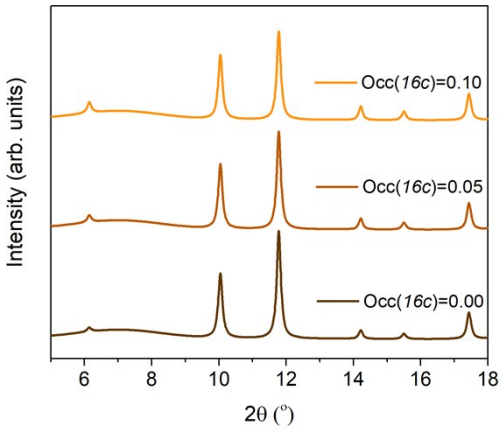

Figure S6. Zoom of Fig. S5.

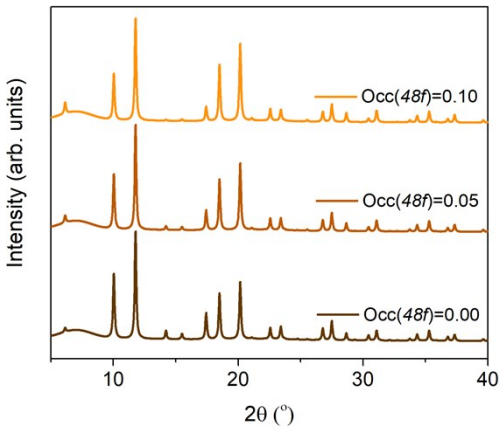

Figure S7. Simulated PXRD patterns for varying degrees of occupancy on the *48f* (0.333, 0.125, 0.125) interstitial site, assuming Zn on the site. The simulations are based on the S1 peak broadening and background description. The occupancy of the interstitial *16c* site is 0. The degree of inversion is set to 0.077% according to ^{27}Al NMR data (Table S1). Occupancy on this site mostly influence the peaks at 6°, 10° and 14.2° relatively to their intensities. These peaks are also highly influenced by the degree of inversion (Fig. S1) and the occupancy on the *16c* site (Fig. S5).

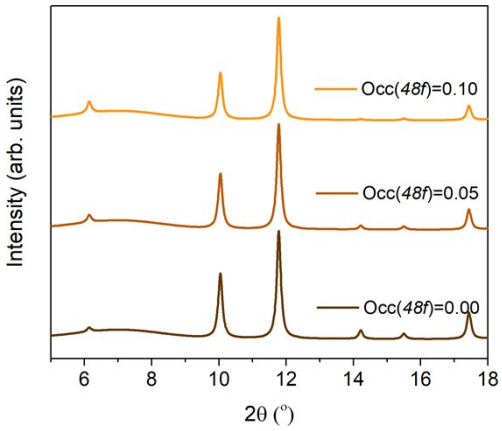

Figure S8. Zoom of Fig. S7.

^{27}Al NMR

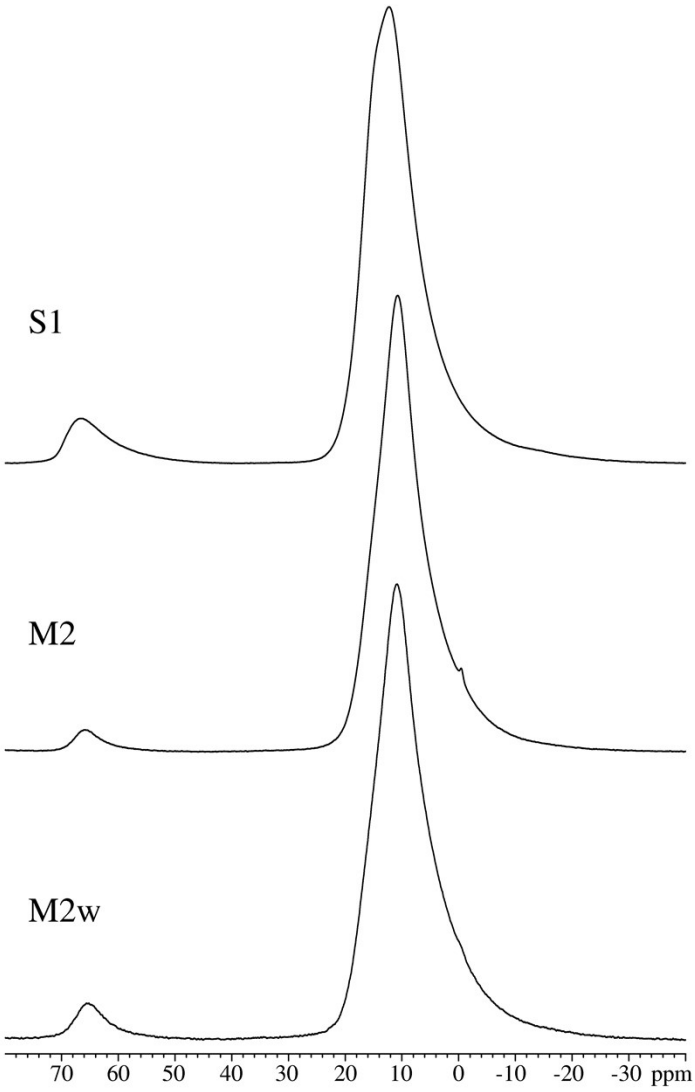

Figure S9. ^{27}Al MAS NMR spectra (14.09 T, ν_R = 13.0 kHz) illustrating the centerbands for Al in tetrahedral (~ 65 ppm) and octahedral coordination (~10 ppm) for the $ZnAl_2O_4$ samples S1, M2 and M2w. The fractions of Al in these coordination states are determined by spectral integration over the centerband peaks.

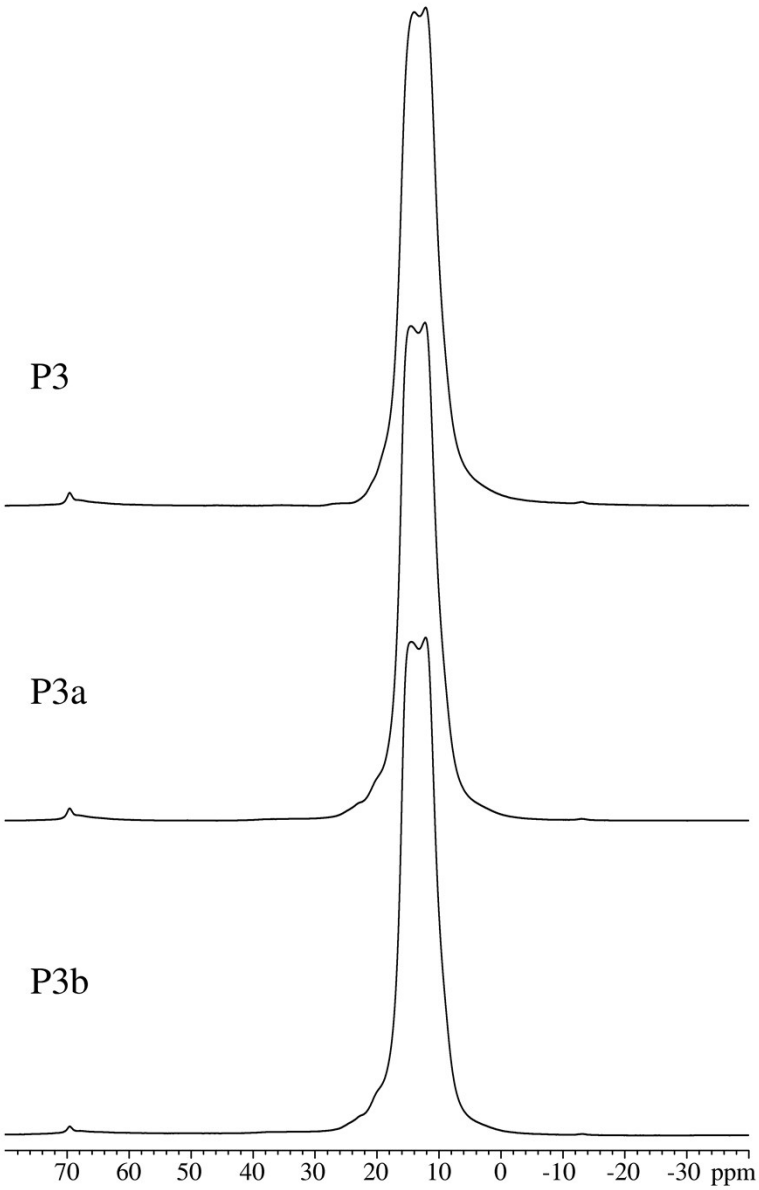

Figure S10. ^{27}Al MAS NMR spectra (14.09 T, ν_R = 13.0 kHz) illustrating the centerbands for Al in tetrahedral (~ 70 ppm) and octahedral coordination (~15 ppm) for the $ZnAl_2O_4$ samples P3, P3a and P3b. The fractions of Al in these coordination states are determined by spectral integration over the centerband peaks. The splitting of the centerband for Al in octahedral coordination reflects the presence of a second-order quadrupolar lineshape and not two distinct Al(6) sites.

.

Table S1. Fractions of Al in tetrahedral (Al(4)) and octahedral (Al((6)) coordination determined from ^{27}Al MAS NMR (Figs. S9 and S10).

Sample	Al(4)	Al(6)
S1	0.077	0.923
M2	0.027	0.973
M2w	0.051	0.949
P3	0.011	0.989
P3a	0.010	0.990
P3b	0.007	0.993

TEM

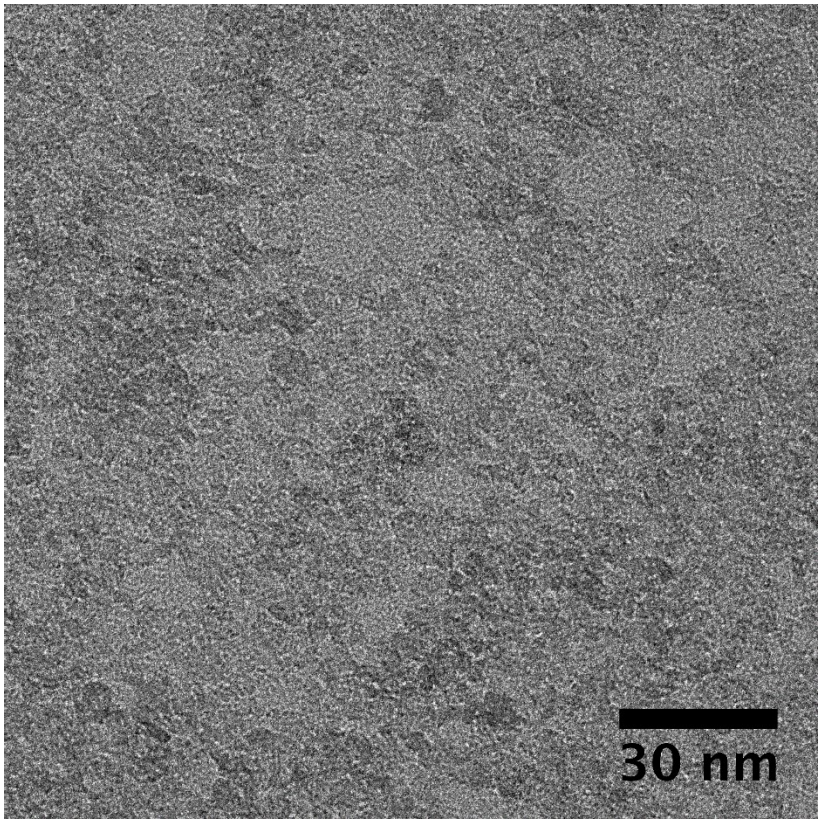

Figure S11. BF-TEM image of sample M2.

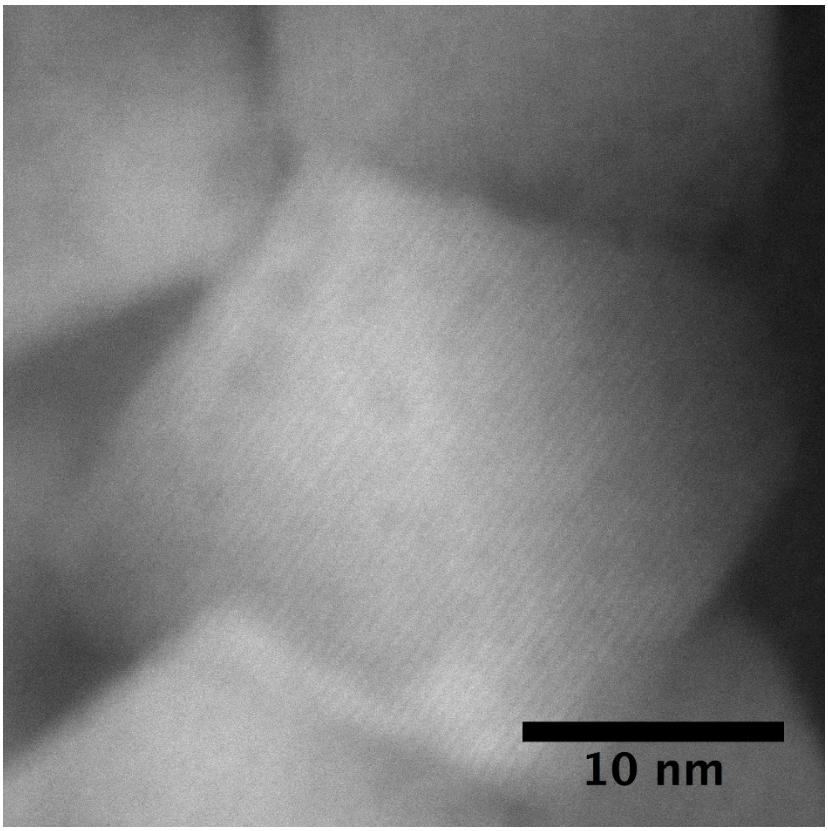

Figure S12. HR-TEM of sample S1.

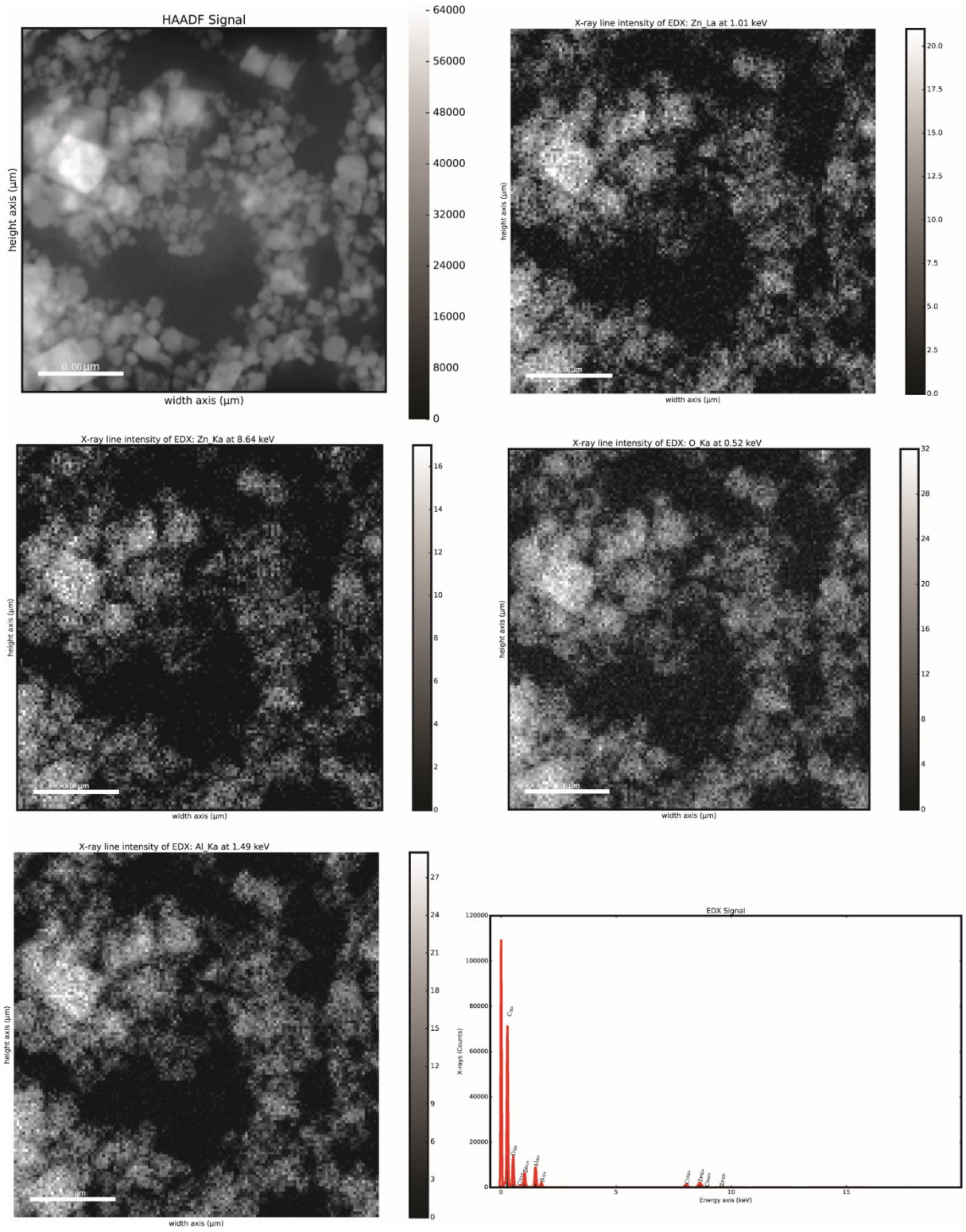

Figure S13. HADDF and EDS images of sample S1.

PDF Simulations

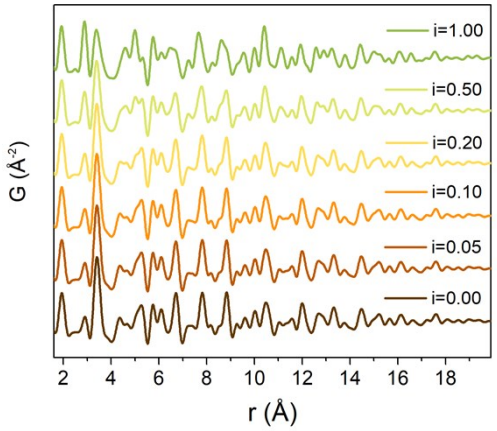

Figure S14. Simulated PDF for various degrees of inversion of the cations, based on the M2w values for particles size, Q_{damp}, Q_{max} and unit cell parameters. The occupancy of the interstitial sites *48f* and *16c* are 0 while the occupancy for oxygen on the spinel *32e* site is 1. The simulations demonstrate how the defects influence the relative peak intensities across the entire simulated r range. Having an incorrect degree of inversion will be observed as a residual across the r range less than the particle size.

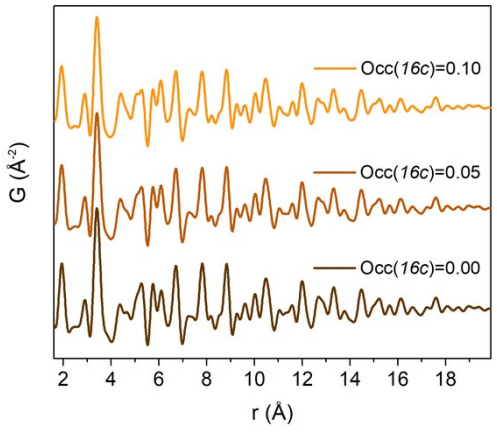

Figure S15. Simulated PDF for varying degrees of occupancy on the *16c* (0, 0, 0) interstitial site, assuming Zn on the site. The simulations are based on the M2w values for the particle size, Q_{damp}, Q_{max} and unit cell parameters. The occupancy of the interstitial *48f* site is 0. The degree of inversion is set to 0.102 according to ^{27}Al NMR data (Table S1). This defect, like the inversion is represented throughout the PDF.

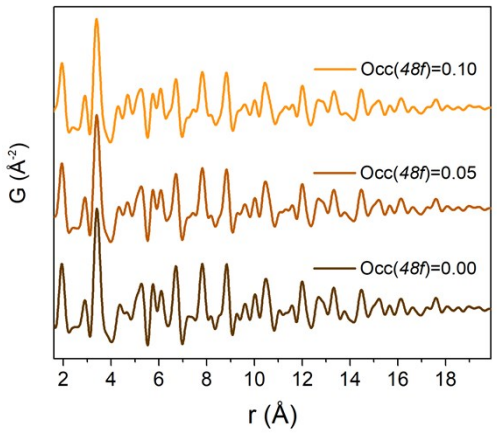

Figure S16. Simulated PDF for varying degrees of occupancy on the *48f* (0.333, 0.125, 0.125) interstitial site, assuming Zn on the site. The simulations are based on the M2w values for the particle size, Q_{damp}, Q_{max} and unit cell parameters. The occupancy of the interstitial *16c* site is 0. The degree of inversion is set to 0.102 according to ^{27}Al NMR data (Table S1). This defect, like the inversion is represented throughout the PDF.

Table S2. PDF analysis of the M2w dataset. The model numbers and remaining parameters corresponds to those provided in Table 2.

Model	i (fraction)	Stoichiometry	Rw
3	0.26(5)	$(Zn_{0.74}Al_{0.26})_{8a}(Zn_{0.26}\ Al_{1.74})_{16d}O_4$	0.257
5	0.25(5)	$(Zn_{0.75}Al_{0.25})_{8a}(Zn_{0.25}\ Al_{1.75})_{16d}(Zn_{0.01})_{16c}O_4$	0.257
6	0.24(6)	$(Zn_{0.76}Al_{0.24})_{8a}(Zn_{0.24}\ Al_{1.76})_{16d}(Zn_{0.01})_{16c}(Zn_{0.14})_{48f}O_4$	0.249
9	^{27}Al NMR constrain of i=0.102	$(Zn_{0.898}Al_{0.102})_{8a}(Zn_{0.102}\ Al_{1.898})_{16d}(Zn_{0.04})_{16c}O_4$	0.264
10	^{27}Al NMR constrain of i=0.102	$(Zn_{0.898}Al_{0.102})_{8a}(Zn_{0.102}Al_{1.898})_{16d}(Zn_{0.160})_{48f}(Zn_{0.03})_{16c}O_4$	0.254

11	Al constrained to ^{27}Al NMR i=0.102 with refined Zn occupancy	$(Zn_{0.93}Al_{0.102})_{8a}(Zn_{0.59}Al_{1.898})_{16d}(Zn_{0.02})_{16c}O_4$	0.244
12	Al constrained to ^{27}Al NMR ratio of $\frac{Al_{tet}}{Al_{oct}} = 0.054$ Zn occupancy	$(Zn_{0.9}Al_{0.2})_{8a}(Zn_0Al_{1.8})_{16d}(Zn_{0.02})_{16c}O_4$	0.254

EXAFS

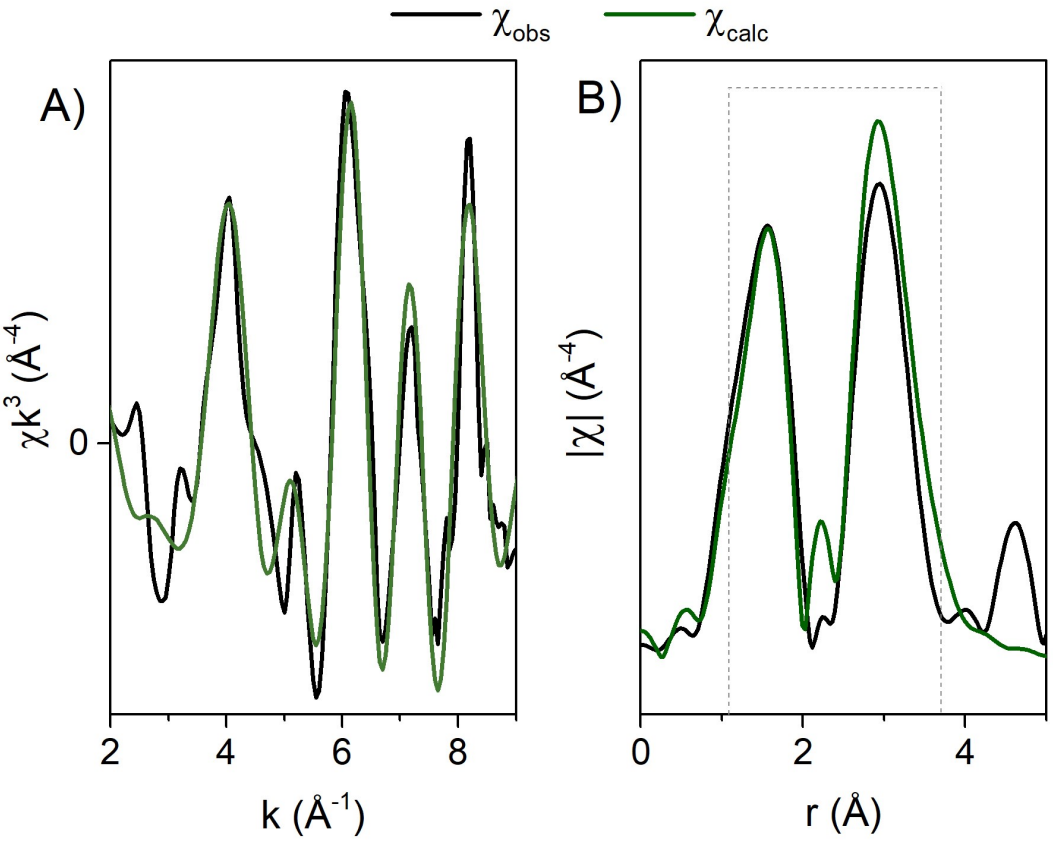

Figure S17. A) Zn-EXAFS modelling in k space of sample M2w from 2 – 9 Å^{-1}. B) the corresponding agreement between the model and the data in real space, including the dashed grey line which indicate the Hanning function.

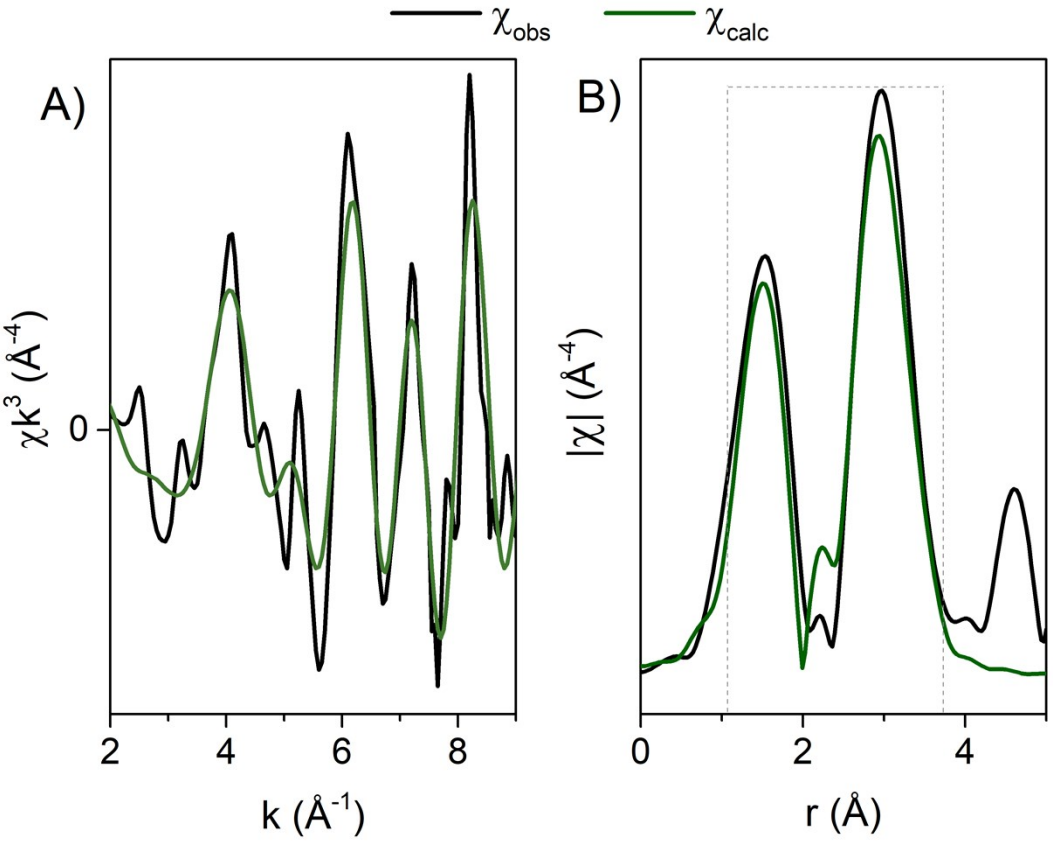

Figure S18. A) Zn-EXAFS modelling in k space of sample S1 from 2 – 9 $Å^{-1}$. B) the corresponding agreement between the model and the data in real space, including the dashed grey line which indicate the Hanning function.

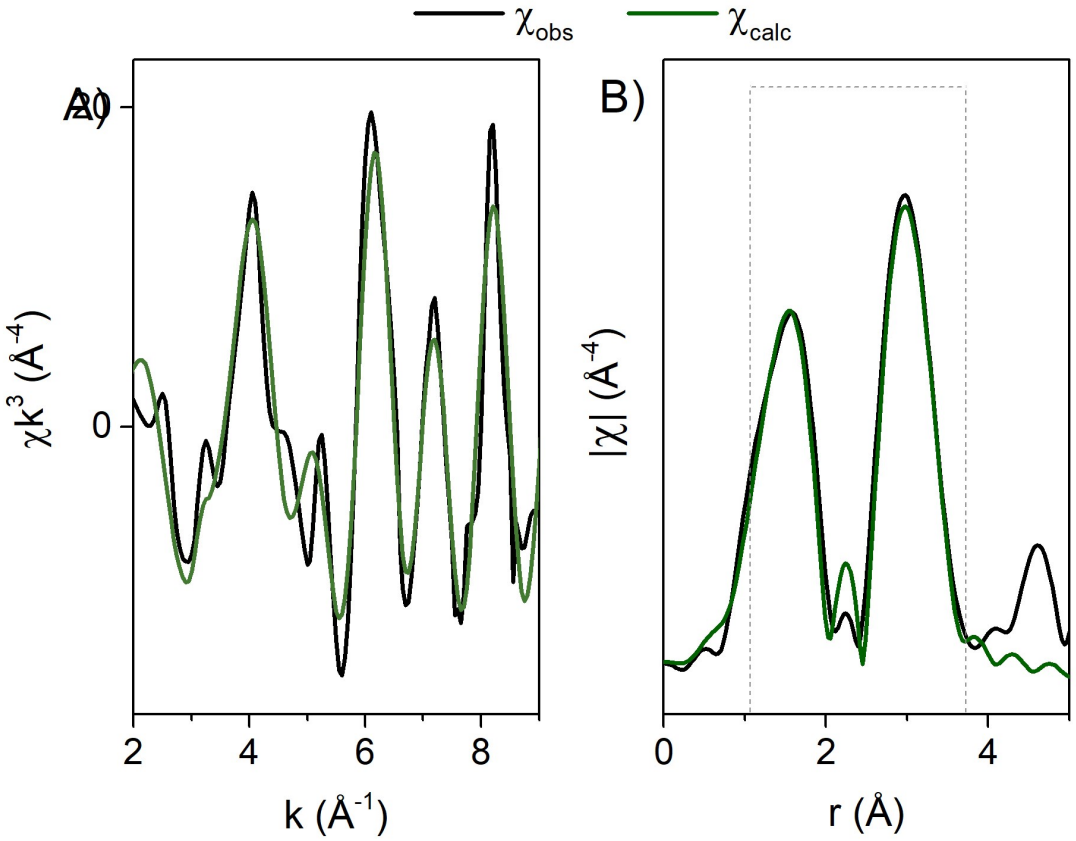

Figure S19. A) Zn-EXAFS modelling in k space of sample M2 from 2 – 9 $Å^{-1}$. B) the corresponding agreement between the model and the data in real space, including the dashed grey line which indicate the Hanning function.

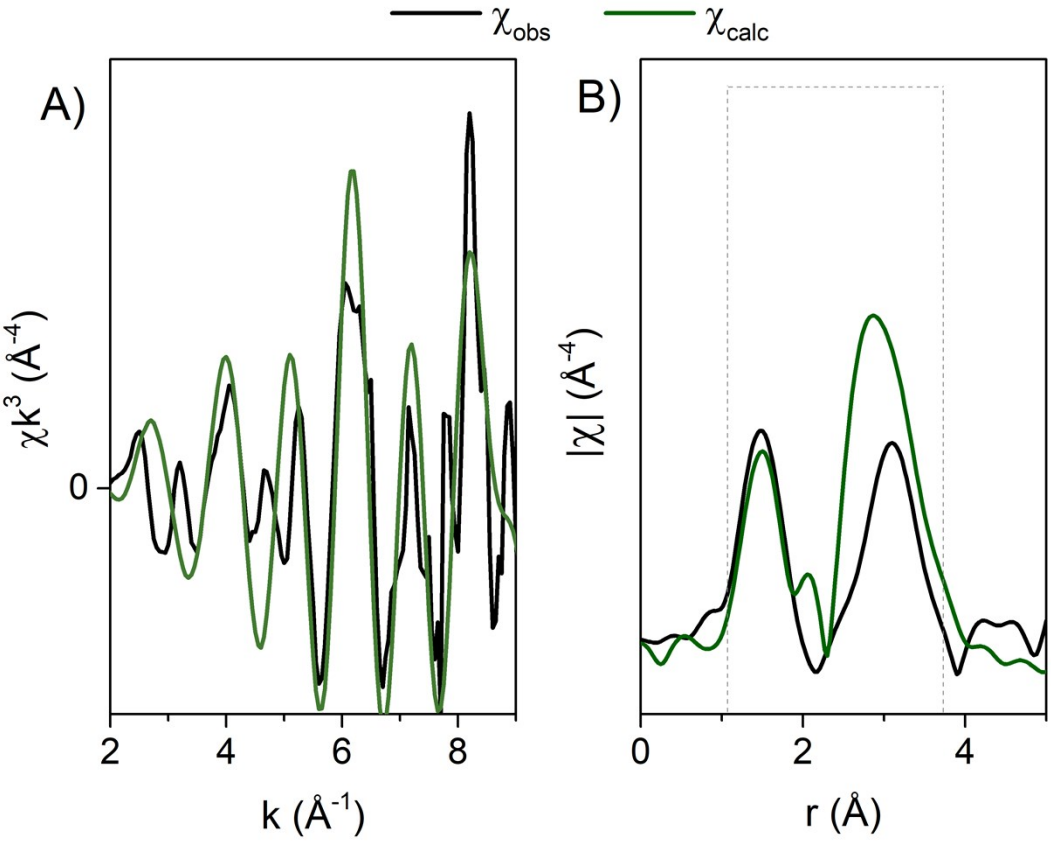

Figure S20. A) Zn-EXAFS modelling in k space of sample P3a from 2 – 9 $Å^{-1}$. B) the corresponding agreement between the model and the data in real space, including the dashed grey line which indicate the Hanning function.

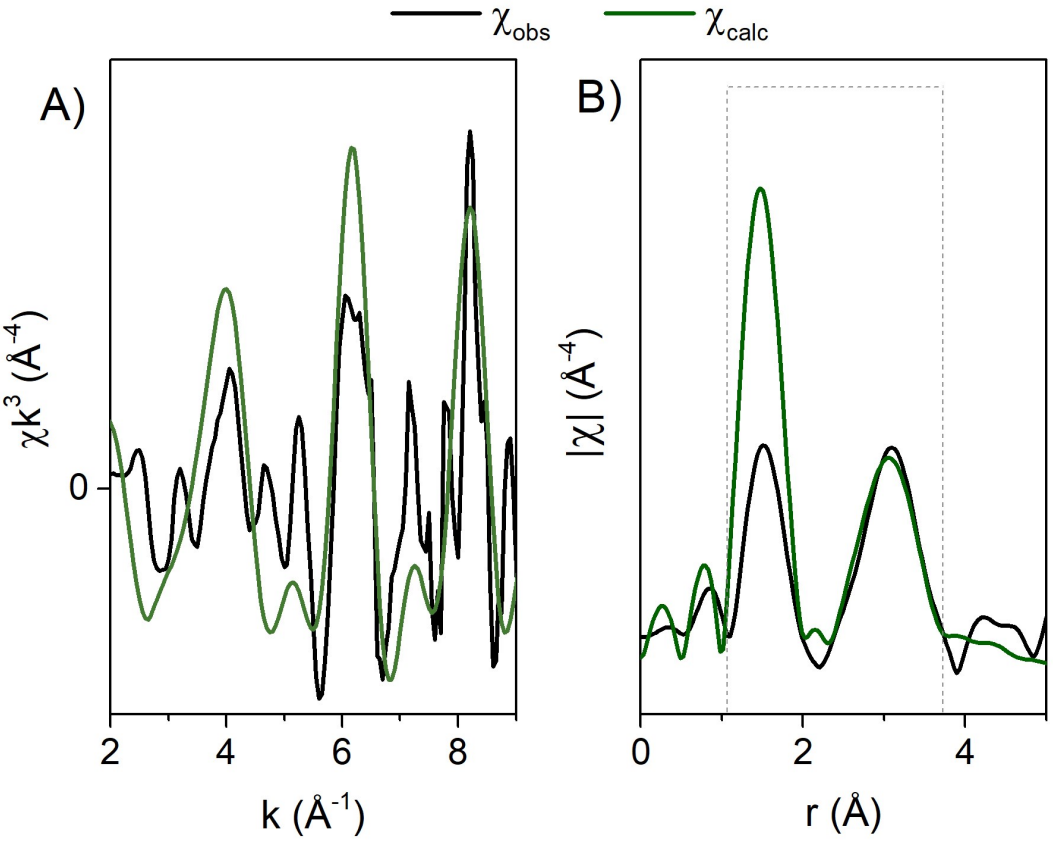

Figure S21. A) Zn-EXAFS modelling in k space of sample P3 from 2 – 9 $Å^{-1}$. B) the corresponding agreement between the model and the data in real space, including the dashed grey line which indicate the Hanning function.

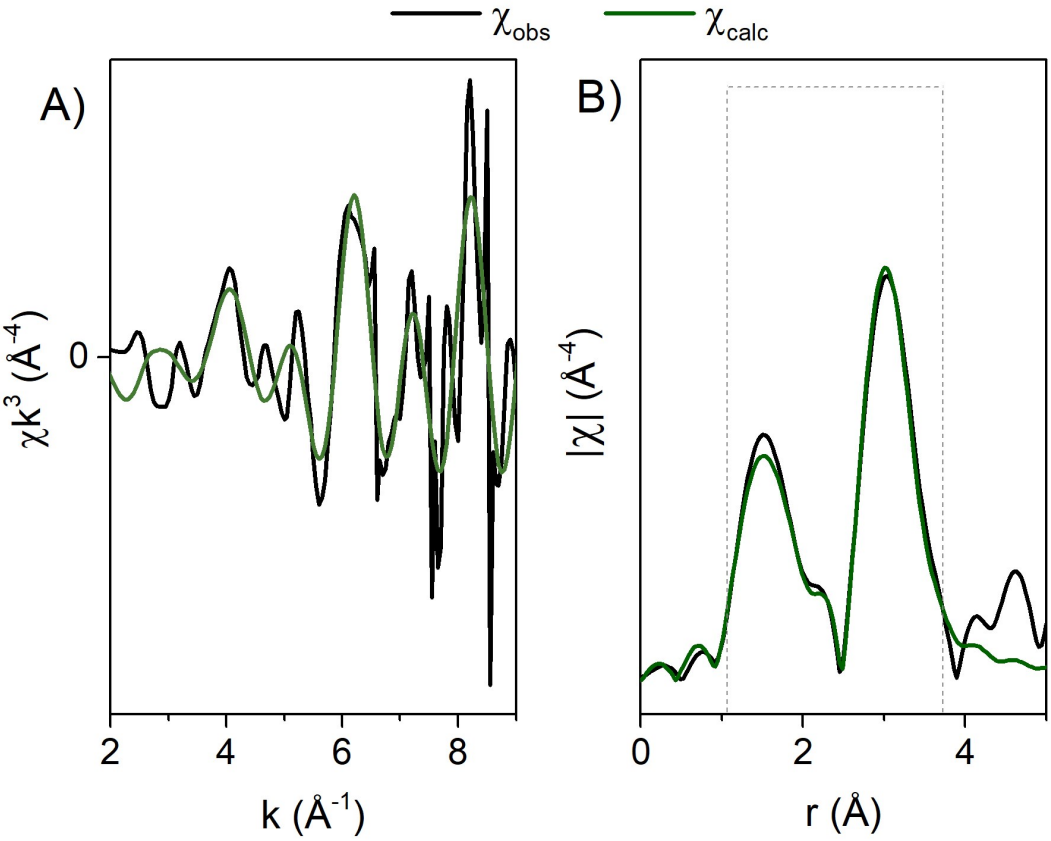

Figure S22. A) Zn-EXAFS modelling in k space of sample P3b from 2 – 9 Å^{-1}. B) the corresponding agreement between the model and the data in real space, including the dashed grey line which indicate the Hanning function.

Table S3. Modelling of Zn-EXAFS data assuming the inversion model.

Sample	**Inversion**	**R-factor**
S1	0.09(3)	0.28
M2	0.067(3)	0.12
M2w	0.32(17)	0.15
P3	0.000(9)	1.04
P3a	0.00(3)	0.77
P3b	0.00(3)	0.47

MEM

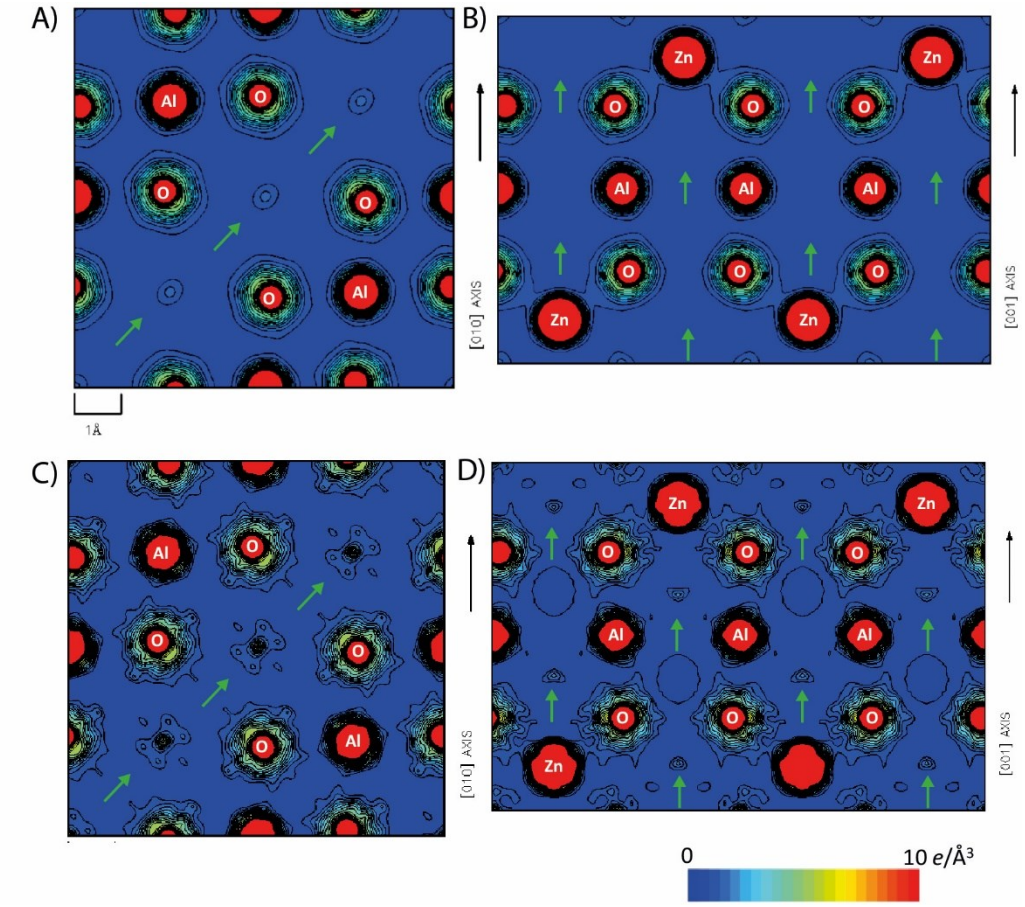

Figure S23. MEM electron density maps of M2 based on Model 1 (A and B) and Model 8 (C and D) . Contour lines are drawn from 0.0 to 2.0 with in steps of 0.2 eÅ^{-3}. The left images represent the [100] plane, while the right images represent [-110]. The calculation with the disorder-free structure models (Model 1) reliability factors were R = 1.04% and R_w = 0.88% while R = 2.28% and R_w = 1.97% for Model 8, where the degree of inversion is constrained to the degree of inversion predicted by ^{27}Al NMR . In both cases residual intensity is observed at the *16c* site while only interstitial intensity at the *48f* site is observed for Model 8. The sites are indicated by green arrows.

PXRD and PDF

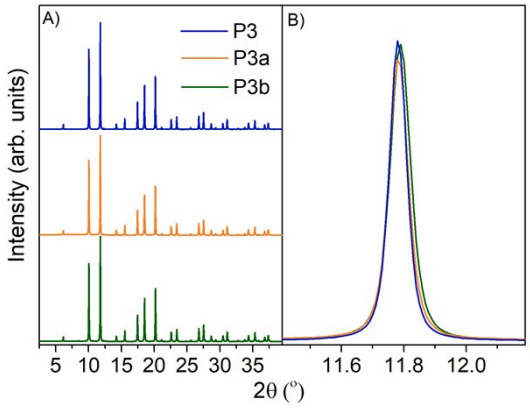

Figure S24. A) PXRD comparison of sample P3 before and after heating to 80 °C for 5 and 7 days (P3a, P3b, respectively). The graph shows that no significant structural changes occur. B) zoom af one peak where the three diffractograms are overlapping. An example af a refinement can be found in Figure 2A. Additionally, it is clear from the PDF refinements that the scattering from the three samples are identical. Extracted parameters are shown in Table 2.

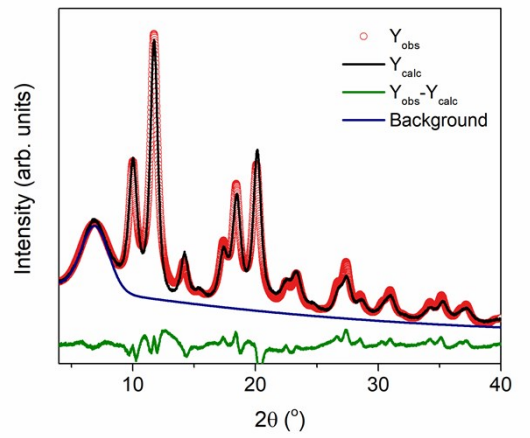

Figure S25. Rietveld refinement of sample M2w heated to 527 °C *in situ*, applying the inversion Model 3 in Table 2.

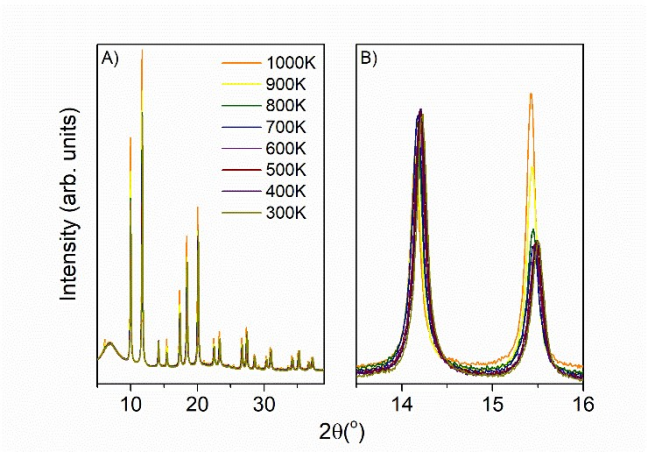

Figure S26. A) *in situ* PXRD of sample S1 during heating. B) zoom in on two selected peaks showing that as the temperature increases the relative peak intensity changes, while the phase remain the same.

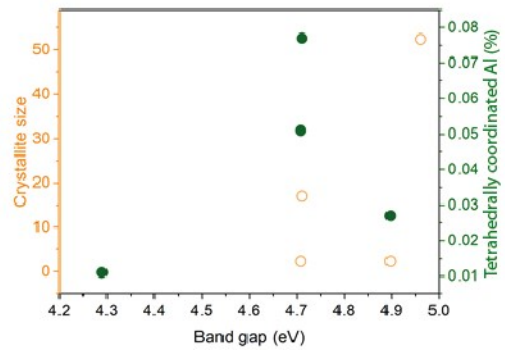

Figure S27. Dual plot of the extracted crystallite size in nm (orange) from Rietveld refinements and the amount of tetrahedrally coordinated Al compared to octahedral coordination based on ^{27}Al NMR (green) as a function of the band gab obtained from DRS-UV-VIS. The samples are S1, M2w, M2, A2 and P3. Sample P3 has crystallites larger than the refinement limit and ^{27}Al NMR has not been conducted on the A2 sample, these have therefore been omitted in the relevant plots.

Table S4. Examples of PXRD refinements using Model 3 in Table 2.

Sample	**Inversion**	**a (Å)**	**R_b/R_{wp} (%)**
M2_300K	0.210(4)	8.106(1)	2.16/2.89
M2_500K	0.233(4)	8.111(1)	2.06/2.78
M2_700K	0.241(4)	8.097(1)	1.98/2.72
M2 900K	0.169(4)	8.077(1)	2.12/3.05
M2_1000K	0.112(4)	8.0945(8)	1.75/3.74

Table S5. Rietveld refined unit cell parameters for the models and samples provided in Table 2.

Model	Sample	$a = b = c$ (Å)
1	P3	8.08879(4)
2	P3	8.088805(4)
3	P3	8.08073(4)
1	M2w	8.1284(6)
3	M2w	8.105(1)
4	M2w	8.1281(4)
5	M2w	8.106 (1)
6	M2w	8.106 (8)
7	M2w	8.104(1)
8	M2w	8.096(8)
9	M2w	8.096(8)
10	M2w	8.1290(4)
11	M2w	8.122(7)
3	M2	8.1170(8)
3	S1	8.08911(6)
3	P3a	8.08498(4)
3	P3b	8.08488(4)

Table S6. Extracted degree of inversion based on Rietveld refinements for the samples not provided in the main text.

Model	**Sample**	**i (fraction)**	**ADP (Å²) (*8a*(tet)/*16d*(okt)/ *32e(*O))**	**Stoichiometry**	**R_{wp}/R_b (%)**
3	M2	0.2102(4)	Fixed (0.00407/0.00353 /0.00470)	$(Zn_{0.849}\ Al_{0.151})_{8a}(Zn_{0.151}\ Al_{1.849})_{16d}O_4$	3.83/2.88
3	S1	0.0004(2)	Fixed (0.00407/0.00353 /0.00470)	$(Zn_{0.998}\ Al_{0.002})_{8a}(Zn_{0.002}\ Al_{1.998})_{16d}O_4$	5.63/ 8.58
3	P3a	0.03669(4)	Fixed (0.00407/0.00353 /0.00470)	$(Zn_{0.963}\ Al_{0.037})_{8a}(Zn_{0.037}\ Al_{1.963})_{16d}O_4$	8.06/5.41